Stem Cell Reports
Article

ISSCR

OPEN ACCESS

# Stem Cell-Derived Human Striatal Progenitors Innervate Striatal Targets and Alleviate Sensorimotor Deficit in a Rat Model of Huntington Disease

Dario Besusso,[1,2,12,*] Roberta Schellino,[3,4,12] Marina Boido,[3,4] Sara Belloli,[5,6] Roberta Parolisi,[3,4] Paola Conforti,[1,2] Andrea Faedo,[1,2,11] Manuel Cernigoj,[1,2] Ilaria Campus,[1,2] Angela Laporta,[1,2] Vittoria Dickinson Bocchi,[1,2] Valentina Murtaj,[6,7] Malin Parmar,[10] Paolo Spaiardi,[9] Francesca Talpo,[9] Claudia Maniezzi,[9] Mauro Giuseppe Toselli,[9] Gerardo Biella,[9] Rosa Maria Moresco,[5,6,8] Alessandro Vercelli,[3,4] Annalisa Buffo,[3,4,*] and Elena Cattaneo[1,2,*]

[1]Department of Biosciences, University of Milan, Milan, 20133 Italy
[2]Istituto Nazionale di Genetica Molecolare "Romeo ed Enrica Invernizzi", Milan, 20122 Italy
[3]Department of Neuroscience Rita Levi-Montalcini, University of Turin, Turin 10124, Italy
[4]Neuroscience Institute Cavalieri Ottolenghi, University of Turin, Orbassano, 10043 Italy
[5]Institute of Molecular Bioimaging and Physiology of CNR, Segrate, Milan, 20090 Italy
[6]PET and Nuclear Medicine Unit, San Raffaele Scientific Institute, Milan 20132, Italy
[7]PhD Program in Neuroscience, Department of Medicine and Surgery, University of Milano - Bicocca, Monza MB, 20900 Italy
[8]Department of Medicine and Surgery, University of Milano - Bicocca, Monza MB, 20900 Italy
[9]Department of Biology and Biotechnologies, University of Pavia, Pavia, 27100 Italy
[10]Wallenberg Neuroscience Center and Lund Stem Cell Center, Lund University, 22184 Lund, Sweden
[11]Present address: Axxam SpA, Openzone Bresso Milan, 20091 Italy
[12]Co-first author
*Correspondence: dario.besusso@unimi.it (D.B.), annalisa.buffo@unito.it (A.B.), elena.cattaneo@unimi.it (E.C.)
https://doi.org/10.1016/j.stemcr.2020.03.018

## SUMMARY

Huntington disease (HD) is an inherited late-onset neurological disorder characterized by progressive neuronal loss and disruption of cortical and basal ganglia circuits. Cell replacement using human embryonic stem cells may offer the opportunity to repair the damaged circuits and significantly ameliorate disease conditions. Here, we showed that *in-vitro*-differentiated human striatal progenitors undergo maturation and integrate into host circuits upon intra-striatal transplantation in a rat model of HD. By combining graft-specific immunohistochemistry, rabies virus-mediated synaptic tracing, and *ex vivo* electrophysiology, we showed that grafts can extend projections to the appropriate target structures, including the globus pallidus, the subthalamic nucleus, and the substantia nigra, and receive synaptic contact from both host and graft cells with 6.6 ± 1.6 inputs cell per transplanted neuron. We have also shown that transplants elicited a significant improvement in sensory-motor tasks up to 2 months post-transplant further supporting the therapeutic potential of this approach.

## INTRODUCTION

Huntington disease (HD) is a monogenetic dominant neurodegenerative condition still orphan of a disease-modifying therapy (Caron et al., 2018). Disease-driving mutations at the *HTT* locus result in expansion of the CAG trinucleotide repeat tract residing at the 5′ end of *HTT* exon 1. Expansions larger than 36 repeats trigger neuronal cell loss that preferentially affects striatal projection neurons (medium spiny neurons [MSNs]) but eventually spread to cortical and subcortical regions, ultimately leading to a progressive and irreversible deterioration of cognitive and motor faculties over a period of 20–30 years (Vonsattel et al., 2008).

Recent technological advancements have promoted the emerging of a number of promising strategies aimed at the attenuation of mutant HTT (mutHTT) expression in an allele-specific or non-specific manner (Tabrizi et al., 2019a; Zeitler et al., 2019). These approaches hold substantial hope for mitigating or delaying disease progression (Tabrizi et al., 2019b); however, the loss of neurons occurring before manifestation of symptoms may reduce the impact of mutHTT-lowering strategies, therefore, complementary therapies must be pursued to secure a successful action against HD.

Regenerative medicine aims to develop strategies that can ultimately lead to functional restoration of the affected tissue. Because of the initial selective vulnerability for striatal neurons in HD, this neurodegenerative condition is particularly suited for cell replacement approaches aimed at mitigating MSN loss. Some attempts at using donor cells derived from whole ganglionic eminence of the human fetal brain were pursued (Lelos et al., 2016; Pundt et al., 1996) but with variable results and limited applicability to the clinical context. Therefore, researchers have since looked into an expandable and more reliable cell source for transplantation. MSN-committed progenitors obtained from *in-vitro*-differentiated human pluripotent stem cells represent a key source in cell replacement approaches. Accordingly, a number of protocols have been developed to capture committed MSN progenitors able to survive *in vivo* and restore target tissue activity (Adil et al., 2018;

Arber et al., 2015; Aubry et al., 2008; Carri et al., 2013; Ma et al., 2012; Nicoleau et al., 2013; Wu et al., 2018).

All these studies, however, have generated MSN-like neurons *in vitro* with different degrees of success and efficiency but none has identified the donor cells by assessing the co-expression of the MSN-unique marker combination DARPP32/CTIP2/GABA, leaving unverified the specific neuronal characteristics of the obtained cell product. Moreover, some of these procedures rely on difficult co-culture system (Aubry et al., 2008) or complex manipulation that includes generation of embryoid bodies (Ma et al., 2012) or sophisticated hydrogel-based 3D systems (Adil et al., 2018); they lack functional validation *in vivo* (Nicoleau et al., 2013) or lacked functional recovery after transplantation (Arber et al., 2015).

The long-term efficacy of this approach requires lasting and extensive integration of the graft-to-host circuits and the graft projections must be able to reach striatal target regions and make synaptic contact with the host cells to restore the compromised networks (Wictorin, 1992). These aspects can be investigated with greater granularity in the larger rat brain with respect to the smaller distant rodent cousin.

Here, we present evidence of therapeutic efficacy of a cell replacement approach that uses human embryonic stem cell (ESC)-derived MSN progenitors implanted into a chemically lesioned rat model of HD. Cells differentiated according to a modified protocol by Carri et al. (2013) and others (Conforti et al., 2018; Faedo et al., 2017) were systematically and longitudinally qualified during the entire *in vitro* procedure. Implanted cells showed high rate of graft survival in the absence of uncontrolled overgrowth as judged by positron emission tomography (PET)/magnetic resonance imaging (MRI) longitudinal monitoring and IHC. Importantly, a proportion of donor cells underwent maturation toward identity of MSNs as judged by DARPP32, CTIP2, and GABA expression. They were also able to integrate into the host tissue by reaching striatal target regions and by receiving synaptic connections as revealed by rabies virus (RV)-based synaptic tracing and confirmed by *ex vivo* patch-clamp analysis. Moreover, short-term behavioral studies using different tasks demonstrated functional recovery in lesion-dependent sensorimotor responses.

## Results

### *Human Striatal Progenitor-Derived Grafts Mature in the Lesioned Rat Striatum and Consist of Medium Spiny Projection Neurons 2 Months after Surgery*

With the aim of exploring the potential efficacy of an hESC-based cell therapy for HD in a preclinical setup, we have exposed the hESC line H9 to a striatal differentiation protocol modified from (Carri et al. 2013) (Figure S1A). Systematic *in vitro* cell phenotyping by immunocytochemistry and high-content qPCR revealed a temporal expression pattern that recapitulates trajectories of human ventral telencephalon development (Figures 1A–1D). The cells, starting from a pluripotent state (Figure S1B), show neuroectodermal fate acquisition with 40% ± 13.7% becoming PAX6-positive by 15 days *in vitro* (DIV) (Figure 1B). Early neurons with ventral telencephalic phenotype increased over time, reaching 30.36% ± 11.28% for CTIP2-expressing cells by 50 DIV, with 13.92% ± 1.91% of total cells being CTIP2/DARPP32 double positive and 6.3% ± 0.8% CTIP2/DARPP32/GABA triple-positive (Figures 1A and 1C). Contamination by neurons with cortical identity was only marginal (Figure S1C). High-content qPCR analysis on 49 different markers confirmed subpallial fate acquisition with subpallial- and LGE-specific markers increasing over time until the end of differentiation. Conversely, the expression of pallial markers picked during early differentiation then declined at 50 DIV (Figure 1D; Table S3).

To test the *in vivo* survival and maturation, we first addressed best *in vitro* maturation time for optimal graft survival 2 weeks after transplantation (data not shown) and accordingly we have selected 20 DIV cells to be grafted unilaterally in the striatum of quinolinic acid (QA)-lesioned athymic adult rats. The transplanted animals were followed up for 2 months and then sacrificed for neuroanatomical analyses. We found robust cell survival with 8,905.23 ± 643.9 human nuclei (HuNu)-positive cells per $mm^2$ that occupied a volume of about 6.53 ± 0.6 $mm^3$ per animal (n = 6).

We then analyzed the expression of markers of immature and mature striatal neurons in $HuNu^+$ grafted cells (Figure 2). Of note, the striatal marker CTIP2 was expressed in about half of all the grafted cells (45.3% ± 1.94%, Figures 2B and 2E), 6.14% ± 0.6% among the grafted cells were positive for the striatal determinants EBF1 (Figures 2A and 2E), while cells coexpressing the more mature marker DARPP32 together with CTIP2, typical of MSNs, were 2.80% ± 0.33% (Figures 2B and 2E), with almost all DARPP32-expressing cells coexpressing the striatal determinant CTIP2. In a few instances, grafted cells differentiated along the interneuronal lineage and expressed interneuronal markers, such as Calbindin (CB) (1.83% ± 0.14%) or Calretinin (CR) (2.61% ± 0.42%) (Figures 2C and 2E). A diffuse positivity for the GABA antigen was visible in the graft area, with 28.2% ± 0.8% of the population displaying a strong staining suggestive of an inhibitory identity (Figures 2D and 2E). A minor proportion of human cells instead progressed along the astroglial lineage and showed glial fibrillary acidic protein (GFAP) positivity (2.14% ± 0.23%; Figure 2E). Moreover, less than 1% of the grafted elements differentiated along the dopaminergic lineage and expressed Tyrosine hydroxylase (TH) (0.91% ± 0.2%; Figure 2E).

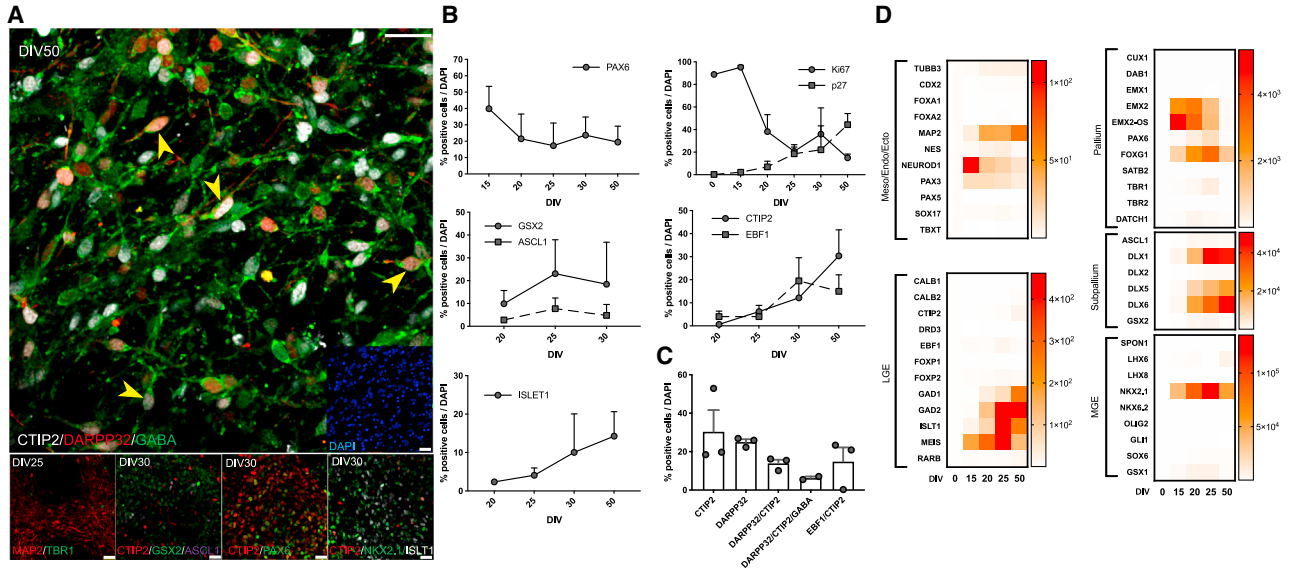


**Figure 1. Cell Phenotyping during *In Vitro* Differentiation Shows Maturation toward the Expected Striatal Cell Lineage**

(A) Representative images showing cell marker expression at different time points during *in vitro* differentiation. Arrowheads indicate triple-positive cells. Scale bar, 25 μm; bottom right inset shows corresponding DAPI staining. Scale bar, 25 μm.

(B) Quantification of relative frequencies of PAX6-, Ki67-, p27-, CTIP2-, EBF1-, ISLET1-, GSX2-, and ASCL1-expressing cells over the total population as defined by DAPI staining during *in vitro* differentiation (mean ± SEM; n = 3 independent experiments, Table S3).

(C) Quantification of cells at the end of differentiation (50 DIV) showing expression of the marker CTIP2, DARPP32, or combination of markers DARPP32/CTIP2, DARPP32/CTIP2/GABA (n = 2 independent experiments), and EBF1/CTIP2 compared with the total population of cells (mean ± SEM; n = 3 independent experiments).

(D) Gene expression of selected region-specific markers at different times during the entire differentiation protocol. Color scale shows $\log_2$ fold change compared with mean expression at 0 DIV for each subset of genes (mean, n = 3 independent experiments; see also Figure S1 and Table S3).

Expression of the neural progenitor marker human NESTIN was still present (67.80% ± 4.5% of HuNu$^+$ cells), indicating incomplete maturation at this time. Nevertheless, we detected relatively few proliferating cells expressing Ki67 (8.69% ± 1.1% of all HuNu$^+$ cells) (Figure 2E).

We also evaluated the occurrence of astrogliosis and microglia activation within the grafts in comparison with either QA-lesioned striata that did not receive the transplanted cells (sham) or to the contralateral unlesioned side (Figure S2). GFAP expression was strongly upregulated by the QA lesion but the graft did not appear to affect GFAP levels (Figures S2A and S2B). Moreover, in the striatum of sham-lesioned animals, microglial cells (IBA1-positive) displayed an overtly activated morphology (Figure S2C), and increased in density, indicating ongoing neuroinflammation. Conversely, upon transplantation, a decrease in microglia activation was observed, although IBA1 levels did not reach the values of the intact unlesioned side (Figure S2D).

Together, these findings demonstrated that the selected striatal progenitors effectively survived the transplantation, progressed in their maturation along the MSN lineage, and partly attenuated ongoing inflammation.

## Transplanted Cells Emit Axons and Project toward Striatal Targets

Axonal outgrowth toward appropriate target regions is essential for the correct reconstitution of the lost circuits and the achievement of long-term therapeutic benefit. To study the dynamics of graft-derived neurite extension, we examined the selective expression of human Neural cell adhesion molecule (hNCAM) in serial sections of grafted rats along the entire rostro-caudal extension of the forebrain and down to the substantia nigra (SN). We distinguished the core of the graft by hNCAM labeling of human neuronal cell bodies, and estimated the areas covered by hNCAM$^+$ fibers as well as the density of hNCAM positivity in the brain section at 1 and 2 months post-transplant (MPT) (Figure 3).

A dense anti-hNCAM staining was observed in the caudate-putamen region both at 1 and 2 MPT, which corresponded to the main graft location (Figure 3A). When we examined the pattern of hNCAM$^+$ fibers outside the core of the transplant, we observed a progressive expansion of hNCAM$^+$ areas within the MSN ipsilateral target regions, such as the globus pallidus (GP) (Figure 3B) and SN pars reticulata (SNpr) (Figure 3D). hNCAM$^+$ fibers also extended to

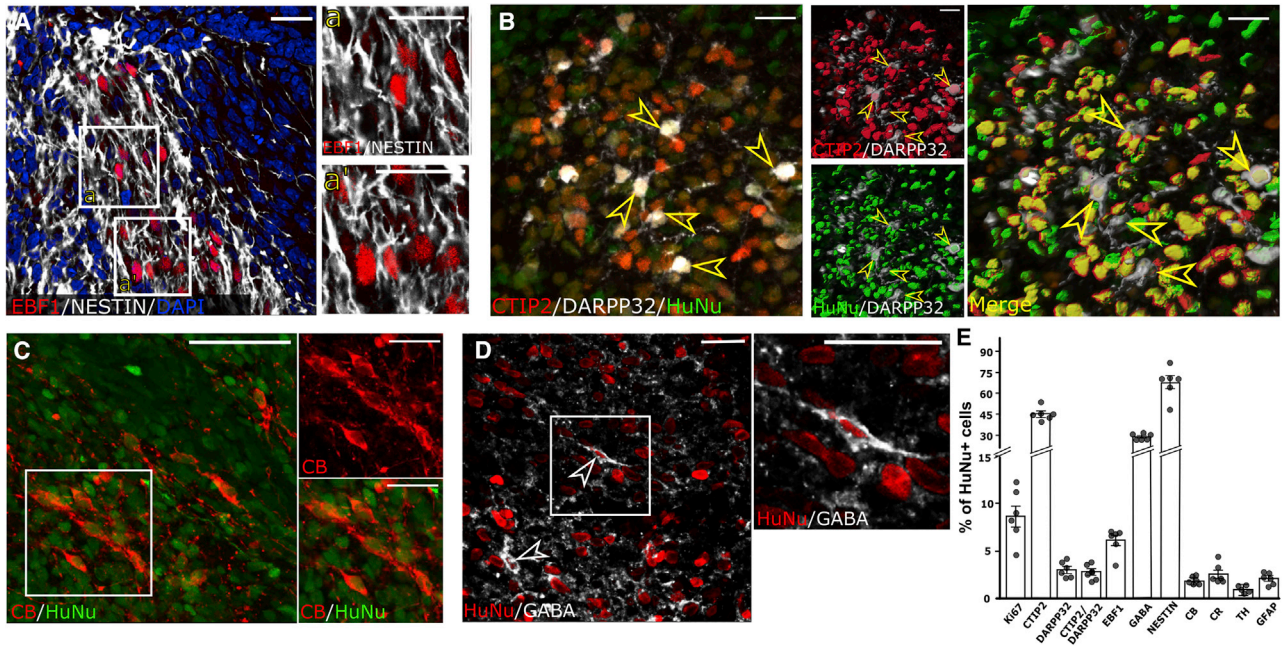


**Figure 2. Maturation of Grafted Cells *In Vivo* Demonstrated Successful Acquisition of Striatal Fate**

(A) Representative graft images showing a fraction of striatal progenitors positive for the NESTIN antigen (NESTIN, white) and EBF1 (red). Insets a and a' show a higher magnification of NESTIN$^+$/EBF1$^+$ cells.

(B) hESC-derived striatal progenitors positive for HuNu mature into MSN neurons expressing CTIP2 and DARPP32. Lateral panels show colocalization through digital rendering. Yellow arrowheads indicate human cells (HuNu$^+$) double-labeled with CTIP2 and DARPP32.

(C) Detail of graft interneurons (green) expressing calbindin (CB) (red).

(D) A diffuse immunopositivity for GABA signal is present in the graft core, with some cells highly marked (white arrowheads).

(E) The graph shows the proportion of cell-type-specific marker expression 2 MPT in HuNu$^+$ neurons. Data are represented as mean ± SEM; n = 6 animals. Scale bars, 20 μm for (A), (B), and (D) and the inset of (C), 50 μm for the main panel of (C).

striatal targets, such as the ventromedial thalamus (VM Th) and the subthalamic nucleus (STN) (Figure 3C). The quantification of the area covered by hNCAM$^+$ fibers showed that, at 1 MPT, rare axonal fibers had reached the SN (Figure 3D), while they were more abundant in the GP and STN (Figures 3B and 3C). However, by 2 MPT, increased hNCAM projections were observed extending along the antero-posterior axis with more fibers in the GP and reaching as far caudal as the SN (Figure 3E).

The increase in fiber extension from 1 to 2 MPT was confirmed by the quantification of the density of hNCAM$^+$ fibers (Figure 3F). In particular, a significant increase in hNCAM$^+$ staining intensity was observed in the VM thalamic region and the SNpr at 2 MPT, compared with the earlier time point, confirming that grafted cells progressively extend neurites that reach target regions anatomically appropriate for striatal MSNs (Figure 3F). Fewer hNCAM-positive fibers were detected to grow toward rostral and dorsal regions. These fibers were found in the ipsilateral (few) and contralateral (rarely) corpus callosum, from where they occasionally reached the lower levels of the motor cortex or the septum (Figure S3). We cannot exclude that they may have been originated by cells occasionally seeded along the injection track.

Overall, these data indicate that processes from the implanted human striatal progenitors expand in the lesioned striatum and project to striatal target regions in a rat model of HD.

## Monosynaptic Tracing Reveals the Formation of Early Host-to-Graft Connectivity

Monosynaptic tracing allows for unambiguous identification of first-order inputs onto a defined population of starter neurons, by taking advantage of the selective retrograde transsynaptic spread of RV. Before grafting, cells were transduced with a lentivirus expressing the rabies helper construct under control of the human synapsin promoter. The tracing construct includes histone-tagged GFP (for unambiguous identification of starter cells); TVA receptor (required for selective primary infection with EnvA-pseudotyped glycoprotein-deleted rabies virus [ΔGRV]); and rabies glycoprotein (required for transsynaptic spread of ΔGRV). One week before sacrifice, transplanted rats received an intra-graft injection of an ΔGRV carrying an mCherry

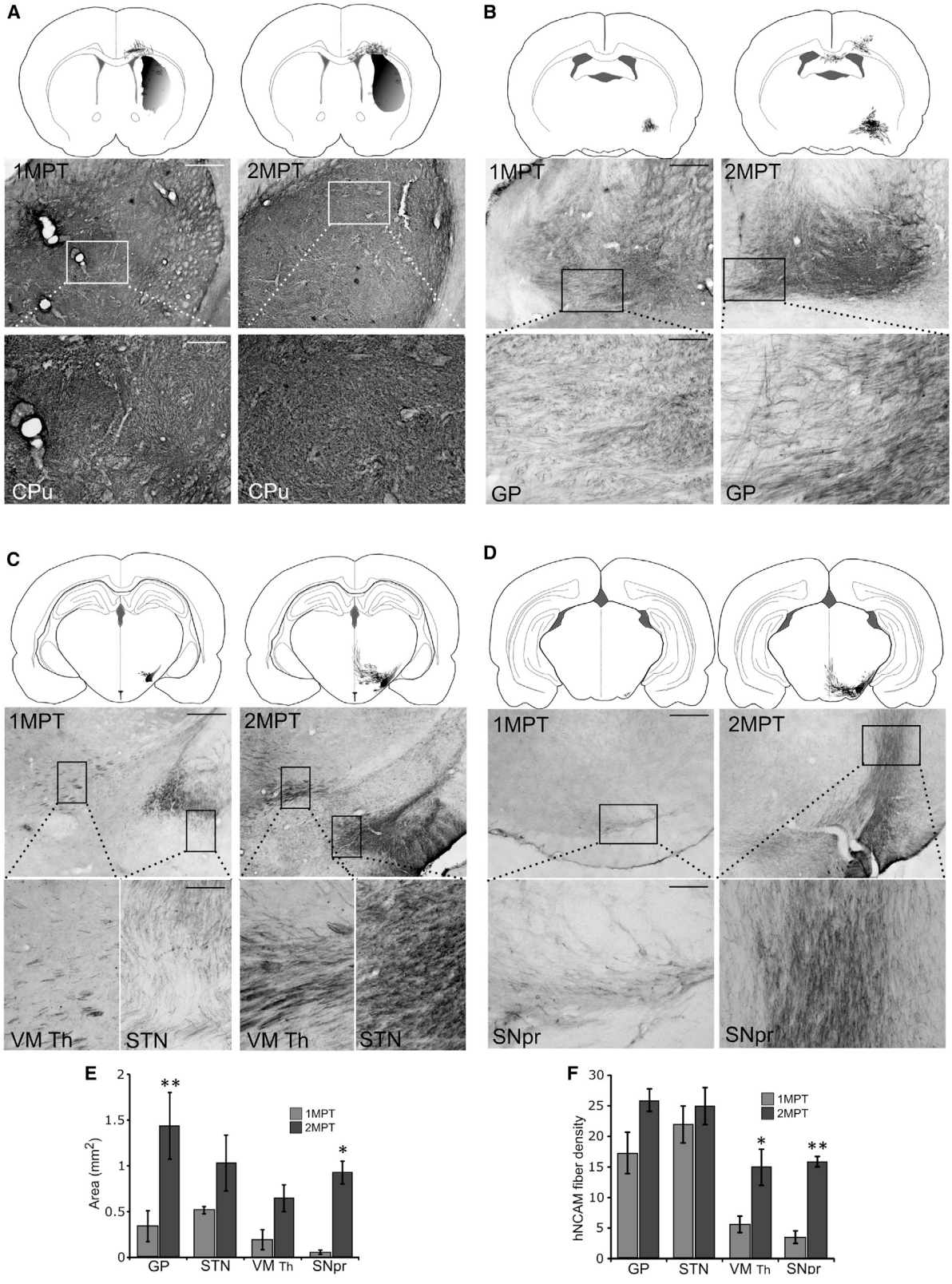


*(legend continued on next page)*

reporter to label first afferent neurons (traced cells) to starter cells belonging to the graft (Grealish et al., 2015).

At both 1 and 2 MPT we found grafted cells identified by nuclear GFP and/or by mCherry as for cells infected by ΔGRV. A fraction of the latter cells corresponded to $GFP^+$ starter cells, while those remaining were first-order afferents, where the ΔGRV had spread transsynaptically (traced cells, $mCherry^+/GFP^-$) (Figures 4A–4D). $mCherry^+$ neurons were localized within the striatum in all examined animals and formed nets with the transplanted cells (Figure 4A, insets a, a'; Figure 4B, insets b, b'). Two months after graft, both the starter and the traced elements were significantly increased within the whole population compared with 1 MPT (Figures 4C and 4E). Interestingly, traced cells increased with time together with a significant increase of the connectivity index (computed as percentage of traced cells over starter cells; 1.5 ± 0.1 at 1 MPT and 6.6 ± 1.6 at 2 MPT; Wilcoxon-Mann-Whitney test, 1 versus 2 MPT, $p < 0.05$; $n = 4$).

Starter neurons were connected with both cells from the graft ($HuNu^+$) and cells from the host ($HuNu^-$) (Figures 4C–4F, S4B, and S4E), showing the initial formation of local synapses and a relevant degree of integration into pre-existing circuits (Figures 4C and 4F). Among traced cells ($mCherry^+/GFP^-$), we found that graft inputs ($HuNu^+$) were predominant both at 1 and 2 MPT (Figure 4F), suggesting that the increase of traced neurons we observed at 2 MPT (Figure 4E) was mainly due to grafted neurons being integrated in newly established intra-transplant networks.

We then characterized the phenotype of the starter and traced cells by analyzing marker expression (Figure S4), and found that a relevant number of $mCherry^+$ cells were marked by CTIP2, while a small proportion showed expression of DARPP32—confirming that a fraction of grafted neurons is further progressing in the MSN lineage—and of interneuron markers (Figure S4A), while more frequently revealing an interneuron identity (Figures 4G and S4D). Over time, a few $DARPP32^+$ neurons also appeared among traced host cells, further supporting progressive integration (Figure 4G). These findings indicate that grafted cells are synaptically integrated and form networks within the graft and with the host circuits.

### In Vivo *Imaging Suggests Graft-Mediated Reduction of QA Inflammatory Response and No Formation of Teratomas*

We decided to monitor the transplants in live animals using clinically relevant MRI and PET imaging techniques. Microglia activation/macrophage infiltration was imaged in QA-lesioned animals using PET and the translocator protein (TSPO) radiopharmaceutical [$^{18}$F]VC701, at 1 week (WPT), 2 MPT, or after sham surgery. At early time point (1 WPT) QA induced a significant increase of [$^{18}$F]VC701 uptake on lesioned striatum compared with the healthy contralateral one, in both sham and transplanted animals (Figure 5A). Conversely, at 2 MPT a significant increase of [$^{18}$F]VC701 uptake in the lesioned striatum was observed only in the sham group (Figure 5B). This result is consistent with that observed by IBA1-staining quantification (Figure S2A) and suggests a role for the grafts in reducing QA-triggered neuroinflammation.

Further analyses of $D_2/D_3$ dopamine receptor availability 2 MPT using [$^{11}$C]RAC as radiopharmaceutical agent did not show any change in $D_2/D_3$-expressing cells in the transplanted striatum compared with sham controls (Figure 5C). To verify if cell transplantation was able to reduce tissue damage induced by QA administration, rats underwent T1-Gd and T2-weighted MRI studies. Gadolinium enhancement was reduced in sham-operated rats and absent in the grafted regions of transplanted animals (Figure S5C and S5D). This suggests a reduction in resident tissue inflammation promoted by the graft and absence of neoplastic transformation or teratoma formation. Finally, sham-operated but not transplanted animals showed enlargements of ventricles in proximity of the QA-lesioned sides, suggestive of a cell loss compensation mediated by the graft (Figures S5A and S5B).

### *Patch-Clamp Recording of Transplanted Cells Reveal Action Potentials and Excitatory Synaptic Inputs*

To investigate whether the transplanted neurons in the grafts were functionally active and integrated into the host

**Figure 3. Axonal Outgrowth from Intra-striatal Grafts of hESC-Derived Striatal Progenitors Shows Targeting of Striatal Target Regions**

Neurites emitted by hESC-derived striatal progenitors were visualized by hNCAM staining and mapped over a schematic representation of rat coronal sections at 1 and 2 MPT.

(A–D) (A) hNCAM fibers increase is observed between 1 and 2 MPT in the GP (B), in the VM Th, and in the STN (C), and in the SNpr (D) of the host brain. For each area, lower panels represent higher-magnification insets.

(E) Area innervated by $hNCAM^+$ fibers at the antero-posterior levels shows the outgrowth and progressive innervation of host brain target structures from 1 to 2 MPT ($n = 4$ animals per group; two-way ANOVA, Bonferroni multiple comparison test: GP, $p < 0.01$; SNpr, $p < 0.05$).

(F) Quantification of $hNCAM^+$ fiber density in the striatal target regions confirms progressive innervation as far caudal as the SN ($n = 4$ animals per group; two-way ANOVA, Bonferroni multiple comparison test: VM, $p < 0.05$; SNpr, $p < 0.01$). CC, corpus callosum; CPu, caudate-putamen; GP, globus pallidus; SNpr, substantia nigra pars reticulata; TRPL, transplant; MPT, months post-transplant; VM Th, ventromedial thalamus; STN, diencephalic subthalamic nucleus. Data are represented as mean ± SEM. Scale bars, 500 μm for the upper panels in (A), (B), (C), and (D); 100 μm for the lower panels (see also Figure S3).

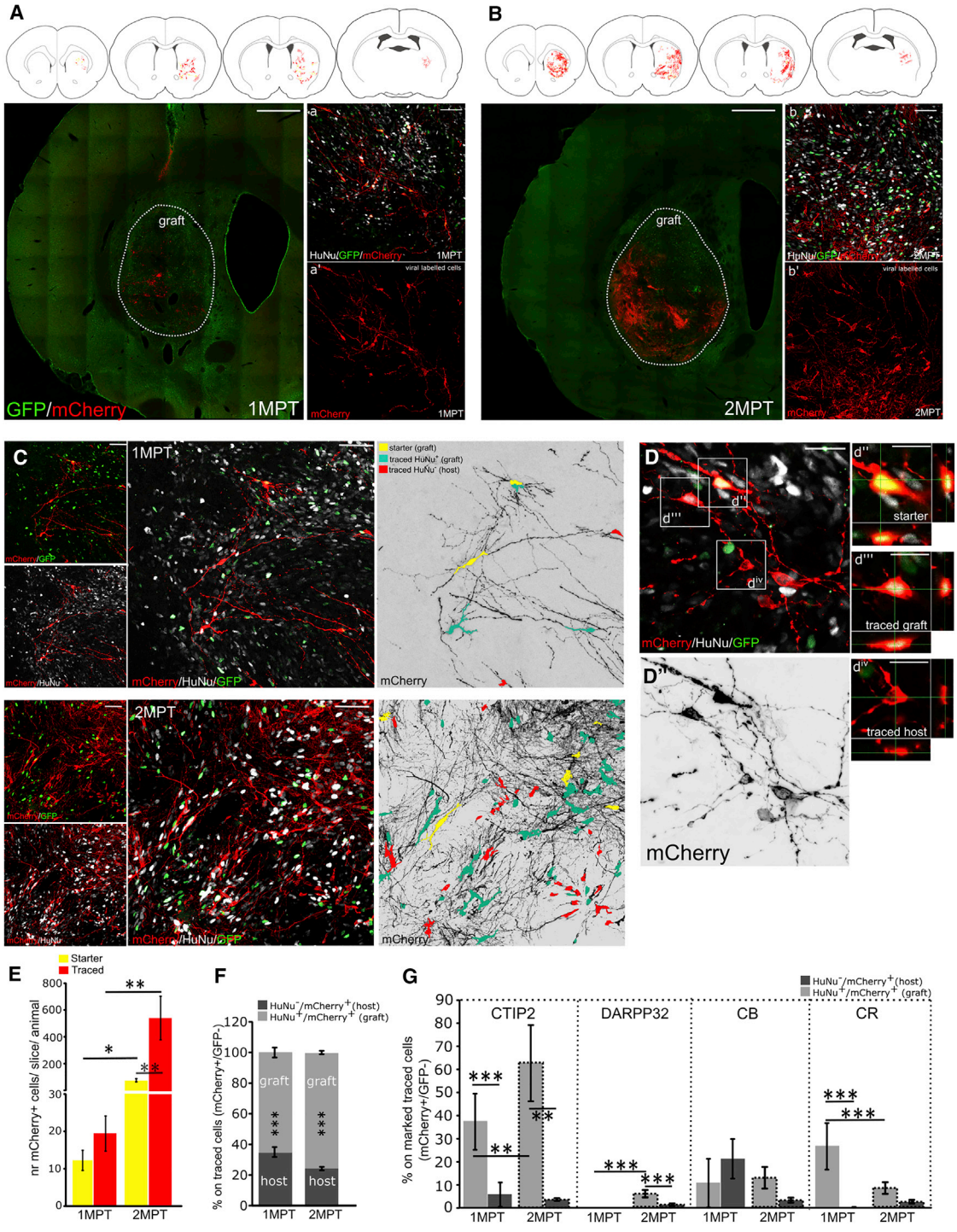


**Figure 4. Host-to-Graft Connectivity of hESC-Derived Neurons is Early Established by Forming Synaptic Connections Preferentially with Interneurons**

Schematic illustration of the antero-posterior distribution of mCherry-positive first-order inputs onto grafted cells in a representative brain at 1 (A) or at 2 (B) MPT. Confocal tile-scan of the entire lesioned hemisphere is presented. The area occupied by the graft is highlighted by dotted line. a, a′ and b, b′ show portions of the graft at higher magnification, in which viral-labeled mCherry-positive starter ($GFP^+$) and traced ($GFP^-$) cells are observed.

*(legend continued on next page)*

brain, we performed 2 MPT patch-clamp recordings on submerged coronal slices, including GFP-labeled grafted neurons. Grafted cells developed a complex dendritic arborization, as observed in cells after labeling with biocytin injection into the cell through the patch pipette during recordings (Figure 6A). Passive membrane properties, an indirect proof of the degree of differentiation, showed that the mean average resting membrane potential of transplanted cells was −55 ± 3 mV, the input resistance was 1801 ± 253 MΩ, and the membrane capacitance was 41 ± 5 pF (n = 26 cells). A distinctive feature of mature neurons is their ability to generate action potentials. Because spike generation is strictly correlated with the expression and activation of voltage-gated TTX-sensitive $Na^+$ and delayed-rectifier $K^+$ channels, we analyzed ionic currents elicited by depolarizing steps during whole-cell voltage clamp. In Figures 6B and 6C, a family of $Na^+$ and $K^+$ currents and action potential firing recorded from a sample of grafted cells are shown, respectively. Overall, in 4% of the recorded cells the amplitude of the peak $Na^+$ current was negligible, 54% of them showed a value smaller than 1,000 pA (mean −391 ± 58 pA)—an arbitrary threshold chosen to define a stem cell-derived mature neuron—whereas the remaining 42% displayed a peak amplitude greater than 1,000 pA (mean −2,655 ± 487 pA) (Figure 6D). Accordingly, in current-clamp mode following supra-threshold stimulation we found that a small fraction of the recorded neurons was able to elicit single (16%) or repetitive (8%) action potentials, whereas the remaining cells showed abortive (36%) or non-regenerative events (40%) (Figure 6E).

The mean peak of $Na^+$ current density, calculated on all tested cells at the peak value of the I/V relationship, was −28.5 ± 5.3 pA/pF (Figure 6F). These data suggest that a portion of grafted cells displayed functional mature neuronal features, i.e., sizable voltage-gated $Na^+$ and $K^+$ currents and the ability to generate action potentials.

Similarly, the voltage-gated $K^+$ current density measured at +30 mV at the steady state gave a value of 988 ± 118 pA/pF (n = 26 cells). Interestingly, 47% of those cells displayed also a fast inactivating outward current component suggesting the activation of an A-type $K^+$ current (Figure 6G).

To explore whether grafted neurons receive functional synaptic inputs (host-to-graft or/and graft-to-graft connections), we recorded spontaneous postsynaptic potentials (sPSPs) at −70mV. Nine recorded neurons out of 25 displayed excitatory sPSPs with an average amplitude of 1.3 ± 0.5 mV (Figure 6H). This result suggests that, at 2 MPT, a subpopulation of grafted neurons begins to show signs of functional integration.

### *Behavioral Assessment of Transplanted QA-Lesioned Rats Shows Improvement in Sensorimotor Responses*

To assess graft-dependent functional recovery, we subjected the transplanted animals to a set of striatum-dependent behavioral tests, including both sensorimotor reflex responses and more complex motor activities. QA lesion clearly worsened the performance of the limb contralateral to the damaged striatum in vibrissae-evoked hand placing (VHPT) and adjusting step test (AST), but had a less-pronounced effect on the general motor behavior (rotarod) in both grafted and non-grafted rats, compared with baseline (Figure 7). In particular, the worsening caused by QA excitotoxicity had a comparable effect in both sham and transplanted rats, and no differences between groups were observed in all tests when rats were examined the day before grafting (7 days after lesion).

In the VHPT, no differences were observed before and after lesion or between sham and grafted rats in the ipsilesional side performance (Figure S6A). On the contralateral side, statistically significant differences were observed between sham and transplanted rats with improved performance in the grafted animals at 1 MPT (Figure 7A). Consistently, at 2 MPT, the performance of grafted rats on the affected forelimb showed a significant improvement to about 190% relative to their postlesion time point ($p < 0.0001$; Figure 7A).

In the AST, no differences were detected between groups in the forward- or backward-adjusting steps

(C) Confocal images representing the distribution of rabies-labeled cell populations. On the right, mCherry positivity is converted into a gray-scale image where starter cells are labeled in yellow, graft traced cells in light blue, and host traced cells in red.
(D and $D^I$) Representative image showing examples of a starter cell ($d^{II}$), and of $mCherry^+$ first afferents belonging to the graft ($d^{III}$) or to the host ($d^{iv}$) with related magnification and re-slice.
(E) Quantification of graft starter and traced cells showing that both cell types increase over time (n = 4 animals per group; $^{**}p < 0.01$, $^{*}p < 0.05$; two-way ANOVA, Bonferroni's multiple comparison test). Data are represented as the average number of $mCherry^+$ cells per slice, per animal.
(F) Quantification of graft or host connections to starter neurons at 1 and 2 MPT (n = 4 animals per group; $^{***}p < 0.001$; two-way ANOVA, Bonferroni's multiple comparison test). Stars inside the bars indicate comparison between $HuNu^+$ and $HuNu^-$ traced cells.
(G) Expression of striatal (CTIP2, DARPP32) and interneuron markers (CR, CB) in labeled $mCherry^+$ inputs, from either graft ($HuNu^+$) or host ($HuNu^-$) cells, 1 and 2 MPT ($^{***}p < 0.001$, $^{**}p < 0.01$, $^{*}p < 0.05$; two-way ANOVA, Bonferroni multiple comparison test). Data are represented as mean ± SEM; n = 4 animals per group.
Scale bars, 1 mm for tile-scan images (A and B); 50 μm for insets a, a′ and b, b′, and for (C); 20 μm for (D) and ($D^I$); 10 μm in $d^{II}$, $d^{III}$, and $d^{IV}$ insets. See also Figure S4.

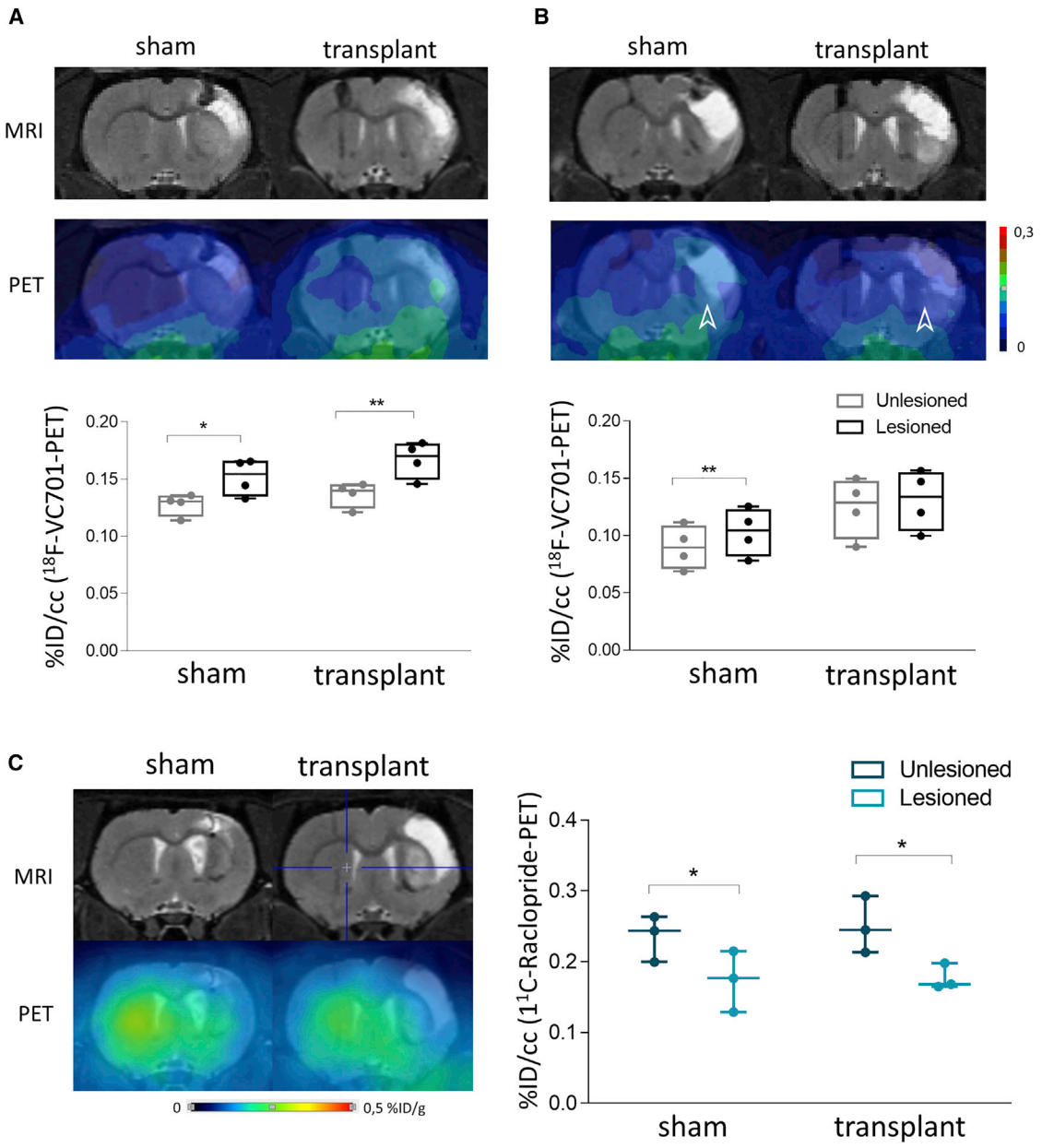


**Figure 5. Longitudinal PET Imaging of inflammation and Dopamine $D_2/D_3$ Receptor Availability**

(A and B) MRI-PET images and PET quantification of $^{18}$F-VC701 tracer uptake 1 WPT, measuring microglial activation in striatal region in both hemispheres (unlesioned and lesioned + transplant) 1 WPT (A) and 2 MPT (B); n = 4 animals per group (*$p < 0.05$, **$p < 0.01$; paired Student's t test); PET images are represented in a "ten-steps" color scale. White arrowheads indicate tracer uptake in the lesioned hemisphere.

(C) MRI-PET images and PET quantification of the [$^{11}$C]Raclopride tracer uptake 2 MPT measuring $D_2/D_3$ receptor availability on the striatal region in both hemispheres, n = 3 animals per group (*$p < 0.05$; paired Student's t test). Data are expressed as percentage of injected dose per volume (mL), mean ± SD.

See also Figure S5.

made using the ipsilateral paw (Figure S6B), while the analysis of the contralateral forelimb revealed a general significant improvement in grafted animals, compared with lesioned only animals, at 1 and 2 MPT (Figure 7B). At 1 and 2 MPT, analyses of the postgraft performance revealed that the affected forelimbs improved to 170% and 130% of the postlesion baseline, respectively ($p < 0.0001$; Figure 7B).

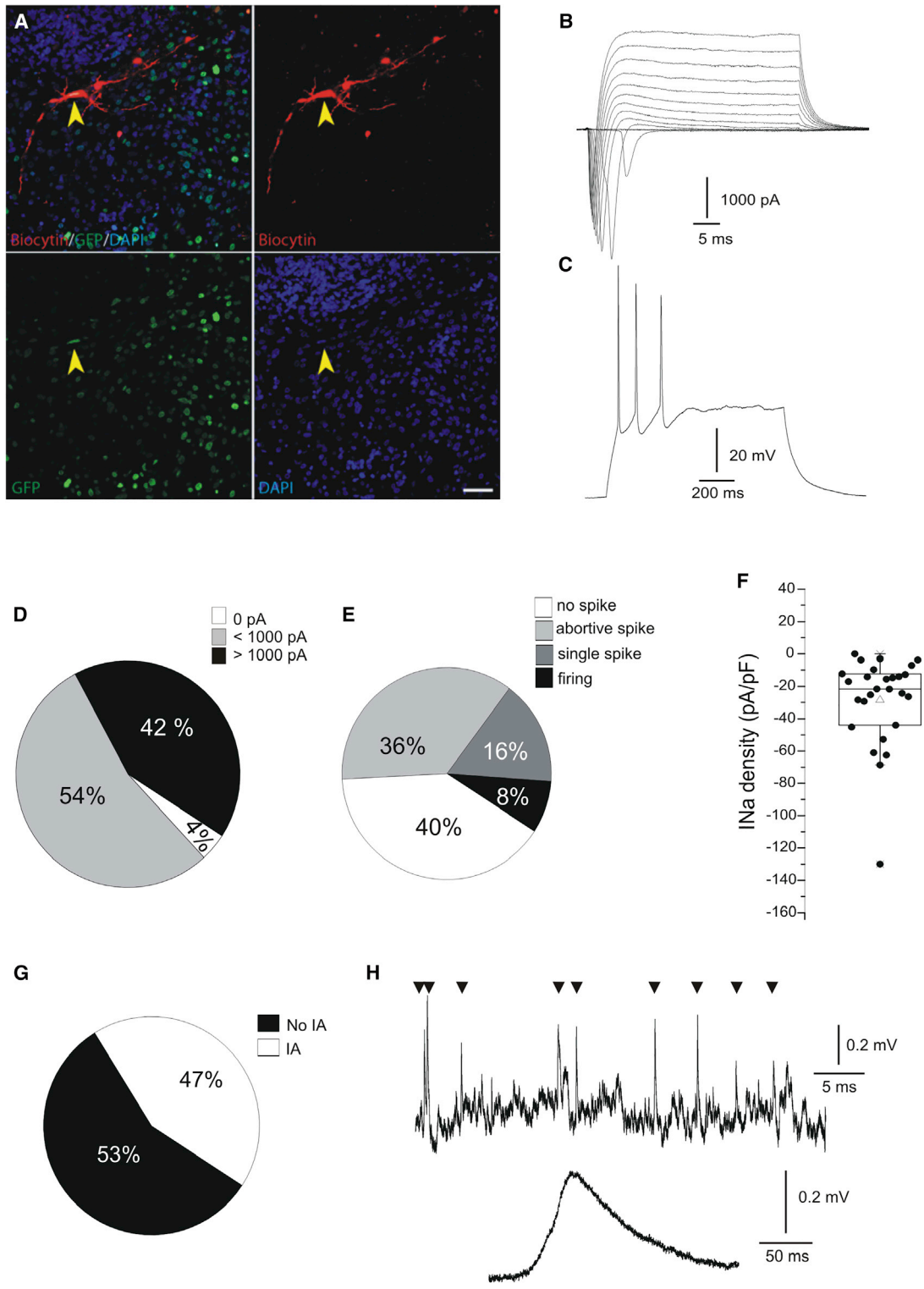


**Figure 6. Transplanted Neurons Generated Action Potentials and Received Excitatory Synaptic Inputs**

(A) Biocytin-labeled patched cell showing complex arborization (arrowhead). Scale bar, 50 μm.

(B) Family of sodium (inward) and potassium (outward) currents elicited by voltage steps from a holding potential of −70 mV.

(C) Sample trace elicited from the same neuron as in (B) showing repetitive firing during stimulation with a supra-threshold depolarizing current step.

*(legend continued on next page)*

Moreover, no differences were observed in the performances on the rotarod between grafted and sham rats, which showed a similar decrease in the latency to fall after lesion (Figure 7C). We also explored the possibility that transplanted cells could provide trophic support to resident MSNs that survived the QA lesion. To this aim, we quantified the density of CTIP2- and DARPP32-expressing rat cells surrounding the lesion site at 2 MPT and found no difference between sham and transplanted animals (Figure S7).

Overall, these data show that hESC-derived neuronal grafts improved sensorimotor reflex responses associated with striatal circuits up to 2 MPT, but failed to rescue more complex motor deficits at these early time points.

## DISCUSSION

In this study, we demonstrated that hESC-derived striatal progenitors, generated *in vitro* through an ontogeny-recapitulating protocol, survive and acquire an MSN identity upon transplantation in a rat model of HD. The grafted cells successfully integrated in the host tissue, establishing early structural and functional synaptic connections, with extended projections reaching proper striatal target regions. Moreover, the transplanted cells ameliorated striatum-dependent sensorimotor deficits in the lesioned rats. Despite these observations, incomplete maturation of the graft was still evident at 2 MPT and no benefits in more complex motor tasks could be detected, facts that are not surprising considering the relative short observational term of the experiments.

Because the emergence of human stem cell technology, a few groups have set up *in vitro* differentiation protocols aiming at generating striatal neurons with features resembling authentic and functional MSNs. Electrophysiological properties and marker expression are the main aspects addressed experimentally to verify the nature of the different cell preparations. Specifically, MSNs are characterized by the expression of markers, including the phosphoprotein DARPP32 and the transcription factor CTIP2, whose expression is, however, shared by other pallial glutamatergic neuronal subtypes (Arlotta et al., 2005). To achieve the unequivocal identification of MSN is, therefore, necessary to leverage their inhibitory nature by assessing simultaneously the expression of GABA or GABA producing enzymes (e.g., GAD65, GAD67).

Here, we have qualified our cell preparations using a systematic approach by assessing the formation of cells expressing key markers during the entire differentiation process. We have identified mature MSNs *in vitro* based on the simultaneous co-expression of the three main markers DARPP32, CTIP2, and GABA. Because of the high level of conservation, no valid human-specific anti-GABA antibody is available in the market, hampering the possibility to perform similar analysis *in vivo*.

For a cell replacement therapy to be effective long-term in HD, the cells generated *in vitro* must be able, upon transplantation, not only to differentiate toward the expected neuronal lineage but also to integrate in the damaged host tissue.

Although previous preclinical works in HD models provided diverse evidence of functional activity of the generated grafts, they have often overseen aspects of connectivity by limiting the analysis to standard-resolution colocalization of synaptic markers found in the proximity of the transplanted cells (Ma et al., 2012) or through EM to show that neural stem cell-derived grafts presumably received both inhibitory and excitatory synaptic inputs from the host without further investigating the source of such contacts (Reidling et al., 2018). Other studies completely neglected these types of analysis leaving the question about transplant integration, unanswered (Adil et al., 2018; Arber et al., 2015; Aubry et al., 2008; Mu et al., 2014; Nicoleau et al., 2013; Wu et al., 2018).

Here, we have extensively investigated the structural synaptic connections that grafts of human striatal progenitors, obtained according to the Delli Carri protocol, were able to establish within the host tissue. By hNCAM staining, we showed that already 1 month after intra-striatal transplantation, grafted cells were able to extend projections reaching striatal target regions, such as GP and STN, with a progressive increase in hNCAM signal from 1 to 2 MPT. Interestingly, some projections were also detected in the SNpr, suggesting that the striato-nigral pathway is potentially reforming early after transplantation.

Furthermore, by leveraging the mentioned RV-based monosynaptic tracing approach (Grealish et al., 2015)

(D) Percentage of cells with peak $Na^+$ currents negligible (white), <1,000 pA (gray), and >1,000 pA (black) (n = 26 cells).
(E) Percentage of cells displaying no spikes (white), abortive spikes (light gray), single spikes (dark gray), and repetitive firing (black) (n = 26 cells).
(F) Boxplot showing the calculated $Na^+$ current density for each recorded cell. Single experimental data are indicated by solid black circles, whereas the mean value is represented by the white triangle (n = 26 cells).
(G) Almost half population of the cells (47%) showed a fast inactivating outward $K^+$ current suggesting the activation of A-type $K^+$ current (n = 26 cells).
(H) Representative trace showing spontaneous excitatory postsynaptic potentials (sEPSPs). The relative mean synaptic event (n = 19 cells), with an amplitude of 0.27 ± 0.09 mV is shown below.

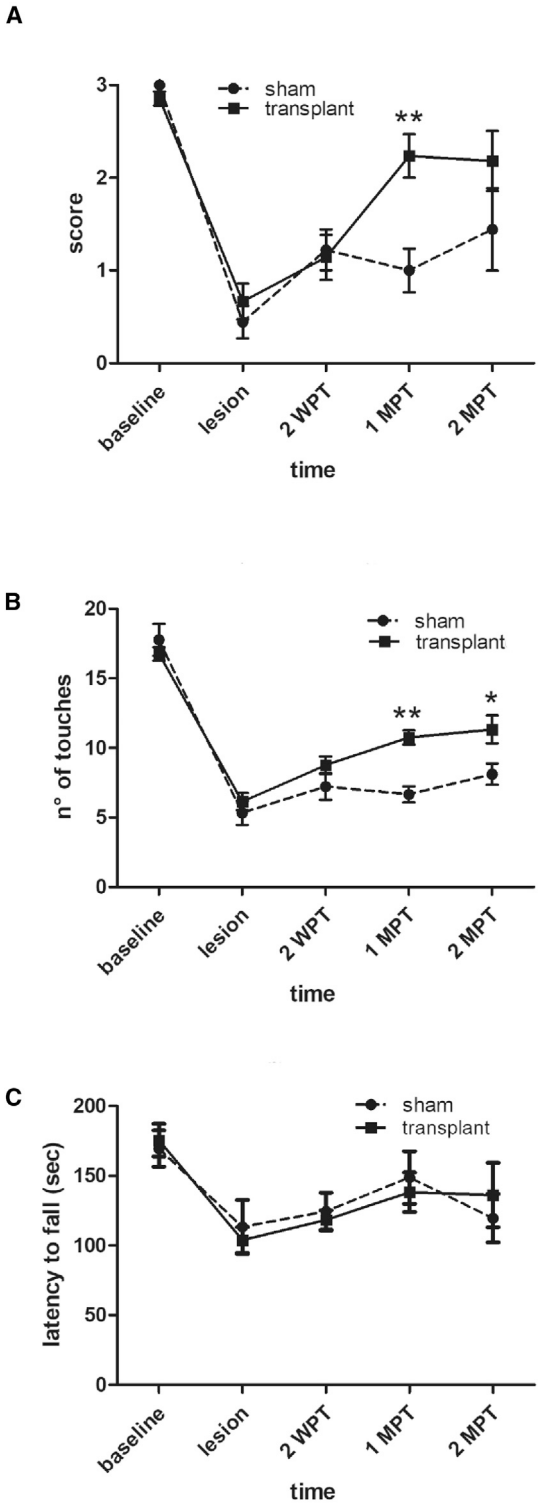


**Figure 7. Intra-striatal Grafts of Striatal Progenitors Alleviated Striatum-Dependent Sensorimotor Deficits**

(A) VHPT showing transplanted rats performing significantly better compared with controls 1 MPT (see Table S4 for details on sample size, two-way ANOVA, Group: $F_{(1;126)} = 6.18$; $p = 0.0142$; Time: $F_{(4;126)} = 24.41$; $p < 0.0001$, Bonferroni multiple comparison test, $^{**}p < 0.01$).

(B) In the AST grafted rats showed a better performance at 1 and 2 MPT ($^{**}p < 0.01$, $^{*}p < 0.05$; two-way ANOVA, Bonferroni multiple comparison test) compared with sham animals.

(C) The rotarod is used to assess sensorimotor coordination before and after the lesion/graft, and the latency to fall from the rotating rod is calculated. No differences were observed in this test between the two groups.

(A and B) Only results related to the contralateral limb are showed (for ipsilateral see Figure S7). Lesion: day before transplant. Data are expressed as mean ± SEM (see also Figure S6 and Table S4 for sample size).

and by quantifying synaptic starter and input cells, we showed that transplanted cells are capable of establishing structural synaptic contacts with both human cells (graft-to-graft) and resident host tissue (host-to-graft). We showed that transplanted cells have greater propensity to connect with surrounding grafted cells rather than with host tissue resident cells, while overall the connection index of starter cells significantly increases from 1 to 2 MPT in line with a progressive increase in network formation.

Moreover, while transplanted cells were shown to be able to make synaptic contacts with resident $CB^+$ interneurons already at 1 MPT, contacts with host $CTIP2^+$ or $DARPP32^+$ MSNs ($mCherry^+/HuNu^-/GFP^-$) only appeared at 2 MPT. This suggests that transplanted cells are capable of reinnervating intra-striatal MSN networks, but this process takes longer compared with connection with host interneurons ($mCherry^+/HuNu^-/GFP^-/CB^+$).

Furthermore, we have been able to detect spontaneous excitatory postsynaptic currents in 36% of the grafted cells at 2 MPT, supporting progressive integration of the grafted cells, and found levels of activation that are to some extent comparable with those found in the literature for endogenous adult rodent tissues.

Interestingly, starting from 1 MPT, grafted animals showed a partial but significant recovery in the impaired forelimb akinesia as detected in both VHPT and AST. Recovery in hand placing upon grafting is particularly relevant, because this deficit is known to persist indefinitely in the presence of extensive striatal damage, such as that induced by QA excitotoxic lesion (Woodlee et al., 2005). The hand-placing amelioration we found is in line with former studies on rat HD models using either rat or human whole ganglionic eminence grafts, which could be considered as the gold standard efficacy reference (Lelos et al., 2016, Klein et al, 2013). Of note, human whole ganglionic eminence grafts were shown to stabilize the impairment in stepping, albeit with no further rescue of the phenotype (Lelos et al., 2016). Hence, grafts of hESC-derived striatal progenitors generated with the Delli Carri protocol appear

more effective compared with whole striatal primordia grafts in promoting recovery of spontaneous sensorimotor responses.

These behavioral improvements nicely parallel the progressive increase in grafted cell connectivity observed by viral tracing techniques and suggest that the newly established circuits participate in integrating sensory and motor information into appropriate striatal outputs. This view is further supported by the dynamic and overall selective outgrowth of neurites from the graft toward appropriate target regions, which well mirrors the capacity of fiber extension shown by rodent and human striatal primordia grafts (Dunnett and Björklund, 2017).

However, conversely with sensorimotor reflex responses, we detected no significant improvement compared with non-grafted animals over time in the rotarod test, which assesses the execution of more complex motor programs and requires the contribution of more complex motor circuits. Additional time may be required to attain the further maturation of the grafted cells, and/or the expansion of the connectivity to cortical and thalamic components potentially required to support these motor tasks.

In summary, we showed that, starting from 1 MPT, stem cell-derived human striatal progenitors grafted into HD rats mature *in vivo*, with a portion of them differentiating into MSNs, while being integrated into local circuits composed of both transplanted and host cells. We show extensive projections of fibers toward appropriate striatal targets with cell differentiation and integration that support the observed functional recovery, although experiments at longer time points are needed to confirm the ability of the graft to sustain long-term complex motor performances.

## EXPERIMENTAL PROCEDURES

### Differentiation of hESCs

hESC H9 were differentiated as described previously with minor modifications described in the Supplemental Experimental Procedures (Carri et al., 2013). For synaptic tracing experiments, 15 DIV and 18 DIV cells were transduced with a synapsin 1-driven TVA-GP-GFP polycistronic lentiviral vector (Addgene no. 30195) with an MOI of 10 in the presence of 4 μg/mL polybrene (Sigma-Aldrich).

### Immunocytochemistry

Cell cultures were fixed in 4% (vol/vol) paraformaldehyde for 15 min at room temperature (RT). Cells were blocked and permeabilized using 5% normal goat serum (Vector), with 0.1% Triton X-100 in PBS for 1 h at RT. After washing, cells were incubated overnight at 4°C with primary antibodies (see Table S1). Next, Alexa Fluor secondary antibodies (Thermo Fisher Scientific) were used 1:1,000 in PBS for 1 h at RT, followed by 3× washes with PBST and 5 min incubation at RT with 1:10,000 of DAPI (Thermo Fisher Scientific) in PBS.

### High-Content qPCR

For high-content qPCR experiments, harvested cDNA was pre-amplified using a 0.2× pool of primers prepared from the same gene expression assays to be used for qPCR. Pre-amplification allows for multiplexed sequence-specific amplification of 29 targets plus 12 reference genes (Table S2). Gene expression experiments were performed using the 96 × 96 qPCR DynamicArray microfluidic chips. Samples and probes were loaded into 96 × 96 chips using an IFC Controller HX, then transferred to a BioMark Real-Time PCR reader following the manufacturer's instructions (Fluidigm).

### Intra-striatal Transplantation of hESC-Derived Progenitors

Athymic NIH FOXN1-RNU nude male rats purchased from Charles River (200–250 g) were lesioned 8 days before transplantation with QA (Sigma-Aldrich) to mimic HD. The lesion was generated by monolateral injection of 210 nmol of freshly made QA into the right striatum using the following stereotaxic coordinates: AP, +0.6; L, ±2.8; V, 5.0 (Ugo Basile). At 20 DIV, hESC-derived striatal progenitors were detached with Accutase (STEMCELL Technologies) with 10 μM ROCK inhibitor (Sigma-Aldrich) and resuspended at a concentration of 50,000 cells/μL. Cells ($3 \times 10^5$) were grafted into the QA-lesioned striata using the following coordinates: AP, +0.9; L, +3.1/–3.1; DV, 5.0. In sham rats, an equivalent volume of PBS was injected in the lesioned striatum.

### Monosynaptic Tracing

One week before perfusion, a set of transplanted rats was injected with EnvA-pseudotyped ΔGRV (a gift from Malin Parmar, Lund University) carrying mCherry reporter to label first afferent neurons (Grealish et al., 2015). For each rat a dilution of 5% of mCherry RV, with a titer of 20–30 × $10^6$ TU/mL, was injected into the lesioned striatum (1 μL total volume) using the same stereotaxic coordinates as for the QA lesion. All surgical procedures were performed under deep general anesthesia obtained with 4% isoflurane (Isoflurane-Vet 100%, Merial Italy) vaporized in $O_2$/$N_2O$ 30%:70%.

### *In Vivo* Imaging

#### *PET Imaging*

PET studies were performed using the high-affinity TSPO radiotracer [$^{18}$F]VC701 to image microglia activation or macrophage infiltration and the D2 dopamine receptor antagonist [$^{11}$C]RACLPRIDE ([$^{11}$C]RAC) to image intra-striatal neurons integrity. PET studies were performed 1 week ([$^{18}$F]VC701) and 2 months ([$^{18}$F]VC701 and [$^{11}$C]RAC) after transplantation. [$^{18}$F]VC701 and [$^{11}$C]RAC were prepared in our facility as described previously (Di Grigoli et al., 2015; Moresco et al., 2008) and intravenously injected into the rat tail vein ([$^{18}$F]VC701, 9.03 ± 1.38 MBq; [$^{11}$C]RAC, 7.49 ± 2.01 MBq).

#### *MRI*

All MRI studies were performed on a 7T preclinical scanner (Bruker, BioSpec 70/30 USR, Paravision 5.1). All rats were prepared for MRI with an intravenous injection of gadobutrol (Gadovist; Bayer Schering Pharma, Berlin) at a dose of 0.05 μmol/g of body weight.

## Behavioral Analysis

All behavioral tests started 1 week before QA lesion to define the baseline performance for each animal. All behavioral tests were conducted blind to the rat treatment(s). The number of animals (sham and transplanted) tested at each time point is reported in Table S4. The following tests were performed:

### *Vibrissae-Evoked Hand Placing*

Rats were lifted upward toward the edge of a table so that only the vibrissae would touch the table edge (Klein et al, 2013). One forepaw is tested while the contralateral one is gently restrained by the experimenter. We recorded the successful movement of the forepaw on the table top and assigned a score from 0 to 3, based on the accuracy of the movement (where 0 corresponds to no movement and 3 to the proper movement), after executing the trial 10 times per side. The test was performed on both the ipsi- and contralesional paws.

### *Adjusting Steps Test*

Forelimb akinesia was assessed using the adjusting steps test (Olsson et al., 1995). This involved restraining one forelimb and counting the number of adjusting steps made by the unrestrained forelimb when a rat was moved sideways along a table surface for 100 cm in either a backward and forward direction with respect to the unrestrained paw. The highest total number of touches per trial was recorded. The data presented are the total number of adjusting steps made with the contralateral and ipsilateral paws.

### *Rotarod Test*

The rats were placed on a rotating rod (Ugo Basile) and steady acceleration was applied (from 4 to 40 rpm in 300 s), and their latency to fall provided a measurement of their motor coordination. The test was repeated for three times per each session and the average latency was recorded.

## Histology and Immunohistochemistry

The cryo-sections were permeabilized with 0.5% Triton X-100 (Sigma-Aldrich) and blocked with 2% donkey serum (Sigma-Aldrich) for 1 h at RT. Next, sections were incubated overnight at 4°C with the primary antibodies at the dilutions indicated in Table S1. Sections were then exposed for 2 h at RT to secondary antibodies conjugated with Alexa Fluor dyes (Thermo Fisher Scientific). hNCAM expression was revealed using the peroxidase technique. Immunohistochemical reactions were performed using the avidin-biotin-peroxidase method (VECTASTAIN ABC Elite Kit; Vector Laboratories) and revealed using 3,3′-diaminobenzidine (3% in Tris-HCl) as chromogen (Sigma-Aldrich).

## Electrophysiological Analysis

Patch-clamp recordings, both in voltage- and current-clamp mode, were performed on submerged slices placed in a recording chamber continuously perfused with carboxygenated artificial cerebrospinal fluid at a flow rate of 0.8–1.3 mL/min. Borosilicate glass patch pipettes were filled with the following intracellular solution: K-gluconate 130 mM; NaCl 4 mM; $MgCl_2$ 2 mM; HEPES 10 mM; EGTA 1 mM; creatine phosphate 5 mM; $Na_2ATP$ 2 mM; $Na_3GTP$ 0.3 mM (pH adjusted to 7.3 with KOH). For a morpho-functional correlation, 3 mg/mL biocytin was intracellularly added through the patch pipette and post-marked by an immunofluorescence reaction after recordings. Electrophysiological recordings were sampled at 20 kHz and filtered at 10 kHz using Clampex 9.2 software and a MultiClamp 700B amplifier interfaced with a personal computer through the Digidata 1322 A/D converter board (all from Molecular Devices, USA). In voltage clamp mode, membrane capacitance ($C_m$) was evaluated by integrating the capacitive current elicited by a −10 mV voltage step, whereas the input resistance ($R_{in}$) was calculated from the same protocol when the signal reached the steady state. Current-clamp recordings were performed to measure the resting membrane potential ($V_r$), the ability to generate action potentials and the presence of sPSPs.

## Statistical Analysis

Data were analyzed using two-tailed Mann-Whitney t test, one- and two-way ANOVA tests, followed by Bonferroni or Dunn's multiple comparison tests for *post-hoc* analyses. Using analysis of variance tests, the between-subjects factor of Group and within-subjects factor of Time were used. PET and MRI data were analyzed using the indicated Student's t test. Results were deemed to be statistically significant when p was <0.05. *$p < 0.05$, **$p < 0.01$, ***$p < 0.001$. See also Table S5 for details.

## SUPPLEMENTAL INFORMATION

Supplemental Information can be found online at https://doi.org/10.1016/j.stemcr.2020.03.018.

## AUTHOR CONTRIBUTIONS

D.B., R.S., S.B., G.B., R.M.M., A.B., and E.C. conceived the study and designed the experiments. P.C., A.F., I.C., and A.L. performed the *in vitro* studies. M.C. helped in producing the lentiviruses. V.D.B. analyzed the high-content qPCR data. R.S. and R.P. performed the transplantation procedures, and histological and behavioral analysis. S.B. and V.M. performed the transplantation procedures and the *in vivo* imaging analysis. P.S., F.T., C.M., and G.B. performed the electrophysiology experiments. M.P. provided the monosynaptic tracing constructs and suggestions on the experimental strategy. All authors contributed to interpretation of the data and their assembly in the manuscript. D.B., R.S., M.B., S.B., G.B., R.M.M., A.B., and E.C. wrote the manuscript and was edited and proofread by all authors. G.B., R.M.M., A.B., and E.C. secured the funding.

## ACKNOWLEDGMENTS

We thank Paolo Provero for helping with statistical analysis, Pia Rivetti Di Val Cervo for helping in the production of viral supernatants, Claudio Cappadona for helping with gene expression normalization and Pasquale Simonelli for the technical support with animal preparation and *ex vivo* experiments.

This work was supported by the Italian Ministry of Research and Education (MIUR) PRIN program (GA no. 2008JKSHKN_001 and GA. no. 2015AY9AYB) coordinated by University of Milan, E.C., and involving University of Torino, University of Pavia, University of Milano-Bicocca and CNR; by the European Union's funded Consortium *NeurostemcellRepair* (FP7 GA no. 602278) and *Nsc-Reconstruct*: *Novel Strategies for Cell based Neural Reconstruction* (H2020, GA no. 875758) coordinated by E.C. and involving A.B. (University of Turin) and M.P. (Lund University). Finally, this work is also

supported by the Italian Ministry of Research and Education (MIUR) national project "Dipartimenti di Eccellenza 2018–2022" awarded to Department of Biosciences (University of Milan), to Department of Neuroscience "Rita Levi Montalcini" (University of Turin) and Department of Biology and Biotechnology "L. Spallanzani", University of Pavia.

Received: October 21, 2019
Revised: March 17, 2020
Accepted: March 18, 2020
Published: April 16, 2020

## REFERENCES

Adil, M.M., Gaj, T., Rao, A.T., Kulkarni, R.U., Fuentes, C.M., Ramadoss, G.N., Ekman, F.K., Miller, E.W., and Schaffer, D.V. (2018). hPSC-derived striatal cells generated using a scalable 3D hydrogel promote recovery in a Huntington disease mouse model. Stem Cell Reports *10*, 1481–1491.

Arber, C., Precious, S.V., Cambray, S., Risner-Janiczek, J.R., Kelly, C., Noakes, Z., Fjodorova, M., Heuer, A., Ungless, M.A., Rodriguez, T.A., et al. (2015). Activin A directs striatal projection neuron differentiation of human pluripotent stem cells. Development *142*, 1375–1386.

Arlotta, P., Molyneaux, B.J., Chen, J., Inoue, J., Kominami, R., and Macklis, J.D. (2005). Neuronal subtype-specific genes that control corticospinal motor neuron development in vivo. Neuron *45*, 207–221.

Aubry, L., Bugi, A., Lefort, N., Rousseau, F., Peschanski, M., and Perrier, A.L. (2008). Striatal progenitors derived from human ES cells mature into DARPP32 neurons in vitro and in quinolinic acid-lesioned rats. Proc. Natl. Acad. Sci. U S A. *105*, 16707–16712.

Caron, N.S., Dorsey, E.R., and Hayden, M.R. (2018). Therapeutic approaches to Huntington disease: from the bench to the clinic. Nat. Rev. Drug Discov. *17*, 729–750.

Carri, A.D., Onorati, M., Lelos, M.J., Castiglioni, V., Faedo, A., Menon, R., Camnasio, S., Vuono, R., Spaiardi, P., Talpo, F., et al. (2013). Developmentally coordinated extrinsic signals drive human pluripotent stem cell differentiation toward authentic DARPP-32$^{+}$ medium-sized spiny neurons. Development *140*, 301.

Conforti, P., Besusso, D., Bocchi, V.D., Faedo, A., Cesana, E., Rossetti, G., Ranzani, V., Svendsen, C.N., Thompson, L.M., Toselli, M., et al. (2018). Faulty neuronal determination and cell polarization are reverted by modulating HD early phenotypes. Proc. Natl. Acad. Sci.U S A. *115*, E762–E771.

Di Grigoli, G., Monterisi, C., Belloli, S., Masiello, V., Politi, L.S., Valenti, S., Paolino, M., Anzini, M., Matarrese, M., Cappelli, A., et al. (2015). Radiosynthesis and preliminary biological evaluation of [$^{18}$F]VC701, a radioligand for translocator Protein. Mol. Imaging *14*, 7290.

Dunnett, S.B., and Björklund, A. (2017). Chapter 1. Mechanisms and use of neural transplants for brain repair. In Progress in Brain Research, S.B. Dunnett and A. Björklund, eds. (Elsevier), pp. 1–51.

Faedo, A., Laporta, A., Segnali, A., Galimberti, M., Besusso, D., Cesana, E., Belloli, S., Moresco, R.M., Tropiano, M., Fucà, E., et al. (2017). Differentiation of human telencephalic progenitor cells into MSNs by inducible expression of Gsx2 and Ebf1. Proc. Natl. Acad. Sci. U S A. *114*, E1234.

Grealish, S., Heuer, A., Cardoso, T., Kirkeby, A., Jönsson, M., Johansson, J., Björklund, A., Jakobsson, J., and Parmar, M. (2015). Monosynaptic tracing using modified rabies virus reveals early and extensive circuit integration of human embryonic stem cell-derived neurons. Stem Cell Reports *4*, 975–983.

Klein, A., Lane, E.L., and Dunnett, S.B. (2013). Brain repair in a unilateral rat model of Huntington's disease: new insights into impairment and restoration of forelimb movement patterns (2113). Cell Transpl. *22*, 1735–1751.

Lelos, M.J., Roberton, V.H., Vinh, N.-N., Harrison, C., Eriksen, P., Torres, E.M., Clinch, S.P., Rosser, A.E., and Dunnett, S.B. (2016). Direct comparison of rat- and human-derived ganglionic eminence tissue grafts on motor function. Cell Transpl. *25*, 665–675.

Ma, L., Hu, B., Liu, Y., Vermilyea, S.C., Liu, H., Gao, L., Sun, Y., Zhang, X., and Zhang, S.-C. (2012). Human embryonic stem cell-derived GABA neurons correct locomotion deficits in quinolinic acid-lesioned mice. Cell Stem Cell *10*, 455–464.

Moresco, R.M., Lavazza, T., Belloli, S., Lecchi, M., Pezzola, A., Todde, S., Matarrese, M., Carpinelli, A., Turolla, E., Zimarino, V., et al. (2008). Quinolinic acid induced neurodegeneration in the striatum: a combined in vivo and in vitro analysis of receptor changes and microglia activation. Eur. J. Nucl. Med. Mol. Imaging *35*, 704–715.

Mu, S., Wang, J., Zhou, G., Peng, W., He, Z., Zhao, Z., Mo, C., Qu, J., and Zhang, J. (2014). Transplantation of induced pluripotent stem cells improves functional recovery in Huntington's disease rat model. PLoS One *9*, e101185.

Nicoleau, C., Varela, C., Bonnefond, C., Maury, Y., Bugi, A., Aubry, L., Viegas, P., Bourgois-Rocha, F., Peschanski, M., and Perrier, A.L. (2013). Embryonic stem cells neural differentiation qualifies the role of Wnt/β-Catenin signals in human telencephalic specification and regionalization: human ESC telencephalic differentiation. Stem Cells *31*, 1763–1774.

Olsson, M., Nikkhah, G., Bentlage, C., and Bjorklund, A. (1995). Forelimb akinesia in the rat Parkinson model: differential effects of dopamine agonists and nigral transplants as assessed by a new stepping test. J. Neurosci. *15*, 3863.

Pundt, L.L., Kondoh, T., Conrad, J.A., and Low, W.C. (1996). Transplantation of human fetal striatum into a rodent model of Huntington's disease ameliorates locomotor deficits. Neurosci. Res. *24*, 415–420.

Reidling, J.C., Relaño-Ginés, A., Holley, S.M., Ochaba, J., Moore, C., Fury, B., Lau, A., Tran, A.H., Yeung, S., Salamati, D., et al. (2018). Human neural stem cell transplantation rescues functional deficits in R6/2 and Q140 Huntington's disease mice. Stem Cell Reports *10*, 58–72.

Tabrizi, S.J., Ghosh, R., and Leavitt, B.R. (2019a). Huntingtin lowering strategies for disease modification in Huntington's disease. Neuron *101*, 801–819.

Tabrizi, S.J., Leavitt, B.R., Landwehrmeyer, G.B., Wild, E.J., Saft, C., Barker, R.A., Blair, N.F., Craufurd, D., Priller, J., Rickards, H., et al.

(2019b). Targeting Huntingtin expression in patients with Huntington's disease. N. Engl. J. Med. *381*, 1398.

Vonsattel, J.P.G., Keller, C., Amaya, Pilar, and del, M. (2008). Neuropathology of Huntington's disease. In Handbook of Clinical Neurology (Elsevier), pp. 599–618.

Wictorin, K. (1992). Anatomy and connectivity of intrastriatal striatal transplants. Prog. Neurobiol. *38*, 611–639.

Woodlee, M.T., Asseo-García, A.M., Zhao, X., Liu, S.J., Jones, T.A., and Schallert, T. (2005). Testing forelimb placing "across the midline" reveals distinct, lesion-dependent patterns of recovery in rats. Exp. Neurol. *2*, 310–317.

Wu, M., Zhang, D., Bi, C., Mi, T., Zhu, W., Xia, L., Teng, Z., Hu, B., and Wu, Y. (2018). A chemical recipe for generation of clinical-grade striatal neurons from hESCs. Stem Cell Reports *11*, 635–650.

Zeitler, B., Froelich, S., Marlen, K., Shivak, D.A., Yu, Q., Li, D., Pearl, J.R., Miller, J.C., Zhang, L., Paschon, D.E., et al. (2019). Allele-selective transcriptional repression of mutant HTT for the treatment of Huntington's disease. Nat. Med. *25*, 1131–1142.